MIDWESTERN

UNIVERSITIES

RESEARCH

ASSOCIATION

DESIGN OF A 50 MEV ELECTRON RADIAL SECTOR FFAG ACCELERATOR

F. T. Cole and A. M. Sessler

REPORT   **NUMBER** 373

DISCLAIMER

This report was prepared as an account of work sponsored by an agency of the United States Government. Neither the United States Government nor any agency thereof, nor any of their employees, makes any warranty, express or implied, or assumes any legal liability or responsibility for the accuracy, completeness, or usefulness of any information, apparatus, product, or process disclosed, or represents that its use would not infringe privately owned rights. Reference herein to any specific commercial product, process, or service by trade name, trademark, manufacturer, or otherwise does not necessarily constitute or imply its endorsement, recommendation, or favoring by the United States Government or any agency thereof. The views and opinions of authors expressed herein do not necessarily state or reflect those of the United States Government or any agency thereof.

DISCLAIMER

Portions of this document may be illegible in electronic image products. Images are produced from the best available original document.

MIDWESTERN UNIVERSITIES RESEARCH ASSOCIATION*

2203 University Avenue, Madison, Wisconsin

DESIGN OF A 50 MEV ELECTRON RADIAL SECTOR FFAG ACCELERATOR

F. T. Cole[+] and A. M. Sessler[++]

November 4, 1957

ABSTRACT: Design considerations and methods used to design a 50 Mev electron radial sector FFAG accelerator are described. Results are given for stability limits and effects of misalignments for various parameters. Design of the magnets to produce the desired field shape is discussed.

I. Introduction

The following is a report on the orbit studies and design work connected with orbits which have been done for a 50 Mev electron FFAG accelerator which is being constructed by the MURA group. It was felt worthwhile to report on this work to ensure that data pertinent to the accelerator would be collected for ready reference and to give for didactic purposes some background for the choice of parameters.

II. Motivation of the Design

The primary purpose of the accelerator is the study of large circulating currents and methods of beam handling with these currents. At the time design studies were begun, the spiral sector FFAG model was not yet operating, and it was felt that the problems of radial sector machines (particularly the non-linear restoring forces) were perhaps more tractable. The use of radial sectors has made possible a further development of the accelerator. By designing the machine with positive and negative field magnets of equal length (called historically a Mark Ia), it is possible by changing the relative excitation of the magnets to make the machine an Ohkawa two-way beam accelerator.[1] Thus experiments can be performed to detect particle collisions and test the principle of colliding beams.[2] The use of Mark Ia rather than Mark Ib (equal magnitudes of fields along the equilibrium orbit in positive and negative magnets) causes the circumference factor to be larger by about one; the circumference factor of the accelerator tuned to the two-way beam position is larger than the optimum Mark Ia by about two.

The desire for high beam intensities influences the design. Experience with the existing radial sector electron model[3] has shown that a generous vertical aperture is necessary to produce high intensities. It is clearly not sufficient, since a large aperture is wasted when the stability limit of vertical oscillations due to non-linear forces is small. One attempts to design for a large vertical stability limit and a correspondingly large vertical aperture, leaving some space for the effects of misalignments.

In addition, rf. acceleration must be used to produce large circulating currents by stacking. Straight sections of minimum length of the order of 8 cm are needed to accommodate rf. cavities. Further, the range of frequency modulation required decreases as the radial aperture decreases, or as

$$k = \frac{r}{B} \frac{\partial B}{\partial r}$$

increases, so that it is desirable to have as high a k as possible.

III. Choice of Energy

In a stacked beam, intensity is limited by gas scattering, which decreases with increasing energy. Enoch[4] has estimated the lifetime of an electron beam against gas scattering. From his results the lifetime is of the order of several seconds at 50 Mev electron energy at a residual gas pressure of 1.4×10^{-6} mm Hg. This will give time for many rf. passes to add particles to the stacked beam. While it would be of great interest for the structure of elementary particles to measure electron-electron scattering at higher energies (of order 200 Mev in each beam), such an accelerator would necessitate a much greater investment in time,

-3-

space and money. At 50 Mev, with a circumference factor of 6 and a maximum field of about 5000 gausses, the outer radius of the accelerator is approximately 200 cm, which will fit reasonably into existing laboratory space.

IV. Computer Methods

The MURA IBM 704 high-speed digital computer has been used extensively* in the design calculations. The methods used are described below.

The "Forocyl" program solves by iteration the magnetostatic problem of the potentials and fields due to given pole and current geometries, inserted as boundary values. Because it was desired to consider various relative positive and negative magnet excitations, the program was used in a particular way. The positive pole was given a potential different from zero and the negative pole was held fixed at zero potential (i.e., not energized). Suppose that this problem gives a median-plane field $B_3^{(1)}$ ($B_r = B_\theta = 0$) whose Fourier expansion at a given radius is (with a particular choice of the zero of θ)

$$B_3^{(1)} = B_0 \sum_n g_n^{(1)} \cos nN\theta \tag{1}$$

Since the negative and positive poles are of equal length, the geometry has period π/N. Then the problem with the negative pole energized and the positive pole at zero has a Fourier expansion

$$B_3^{(2)} = B_0 \sum_n g_n^{(2)} \cos nN\theta = -B_0 \sum_n g_n^{(1)} \cos nN(\theta + \pi/N)$$

$$= -B_0 \sum_n (-1)^n g_n^{(1)} \cos nN\theta . \tag{2}$$

---

*It has been estimated that approximately 600 hours of computer time have been used in this design work.

The problem with the positive and negative poles having relative excitation a/b has a Fourier expansion

$$B_3 = B_0 \sum_n g_n \cos n N\theta = \frac{B_0}{a+b} \sum_n \left(a g_n^{(1)} + b g_n^{(2)} \right) \cos n N\theta$$

$$= \frac{B_0}{a+b} \sum_n g_n^{(1)} \left(a - (-1)^n b \right) \cos n N\theta. \tag{3}$$

With this device it is not necessary to do more than one lengthy Forocyl problem in order to treat various excitations of the same geometry.

The Fourier coefficients of (3) could be used in the "Well-Tempered Five" dynamical program,[6] which generates the fields affecting particle motion at each integration step from the median-plane fields by Powell's expansion.[7] However, the "Formesh" dynamical program,[8] which uses the fields given at points of a mesh (as in Forocyl) has the advantage of greater speed, as well as several useful auxiliary programs, such as "Forfixpoint"[9] and the several bump programs.[10] A field mesh can be made from the Fourier coefficients of (3) by the "Tempermesh" program,[11] which generates the fields as in "Well-Tempered Five" and stores them at mesh points.

The normalization of the Fourier coefficients must be considered further. For radial sector machines, the maximum field on a circle is large compared to the average field and the "scalloping" of the equilibrium orbit makes large contributions to the average field on the equilibrium orbit. This moves the equilibrium orbit to a smaller average radius. The computer programs use variables scaled with respect to a reference radius which is frequently too

large for radial sector machines. Then the interesting dynamical region is far to the left of the origin of the phase plane for radial motion, so that it is easy to exceed scaling limits for the variables. However, this dynamical region can be moved arbitrarily along the x-axis by proper normalization of the Fourier coefficients. The radial equation of motion in the median plane can be written in cylindrical coordinates as

$$\frac{d}{d\theta}\left[\frac{\dot{r}}{(r^2 + \dot{r}^2)^{1/2}}\right] = \frac{r}{(r^2 + \dot{r}^2)^{1/2}} - \alpha\left(\frac{r}{r_0}\right)^{k+1} \sum_n g_n \cos n N \theta , \tag{4}$$

where $\dot{r} = dr/d\theta$ and

$$\alpha = e r_0 B_0 / c p . \tag{5}$$

p is the total particle momentum and the field in the median plane is

$$\begin{cases} B_r = B_\theta = 0 \\ B_3 = -B_0 \left(r/r_0\right)^k \sum_n g_n \cos n N \theta . \end{cases} \tag{6}$$

α defines the circle (of radius r_0) about which the motion is expanded.[12] Since for a given B, r and θ, B_0 varies as r_0^k, α varies as r_0^{k+1}. Thus α_0 and α_1 (of the same sign) corresponding to circles of radius r_0 and r_1 respectively are related by

$$\alpha_1 / \alpha_0 = \left(r_1/r_0\right)^{k+1} . \tag{7}$$

The computer programs use $\alpha = 1$ throughout, but because α appears in the equations of motion multiplying the field, one can insert αg_n rather

than g_n in "Tempermesh" and thus expand about the circle of radius correspond-

ing to α. In practice, initial values of α were found from analytical theory[13]

and improved from the computer results, using (7).

The circumference factor C can also be calculated by using α. It is

defined as

$$C = r_e / \rho_{min} \, ,$$

(8)

where ρ_{min} is the minumum radius of curvature of a particle of momentum p

and r_e is the radius of its equilibrium orbit at the azimuth where $\rho = \rho_{min}$.

Now

$$\rho_{min} = cp / e B_{max}.$$

$$= r_o B_o / \alpha_e B_{max} ,$$

so that

$$C = \alpha_e B_{max} / B_o \, ,$$

(9)

where α_e is that value of α such that $r_o = r_e$. In the radial sector

machines considered in the present work, the minimum of ρ will occur at

the center of a positive magnet, which is taken as $\theta = 0$. Then

$$C = \alpha_e \sum_n g_n \, .$$

(10)

V. Choice of N, k and Geometry

The number of sectors N and k are related choices. In order to have

$\sigma_x < \pi$, it is necessary that $2 \nu_x < N$. From the smooth approxima-

tion

$$\nu_x \gtrsim \sqrt{k+1},$$

so that

$$k \lesssim \frac{1}{4}N^2.$$

(11)

For the present machine k should be as large as is practical, which puts a lower bound on N. However, as N increases, the straight section length available at a given radius decreases. Some exploration was done, beginning with N = 20. It was found that the working points for all two-way machines with N = 20 are slightly below the serious essential coupling resonance $\sigma_x + 2\sigma_3 = 2\pi$. (As shown by Ohkawa,[13] all working points for two-way machines lie essentially in hyperbolae which are functions only of N.) Working points for N = 18 were slightly above this resonance, so that it seemed desirable to go lower. However, N = 14 gave values of k for stable motion ($\lesssim 6$) which were held to be too small by those concerned with rf. systems. N = 16 seemed to offer a reasonable compromise among all these factors.

To find a reasonable geometry and k, various Forocyl problems and dynamics from them were computed. These exploratory problems did not include the effects of finite cross-sectional area of the backwinding return currents. It was desired to find working points for both one-way and two-way operation (with the same geometry and k) which were not too close to misalignment resonances known to be harmful and which had large stability limits against essential non-linear resonances. No systematic investigation was undertaken, because reasonable working points were found with little difficulty.

A geometry giving good results is shown in Fig. 1. This diagram shows pole configurations at a particular radius (the pole shapes being assumed to scale with radius). Half of the positive pole is shown at each edge, with the negative pole in the center, so that $\theta = 0$ at the center of the positive magnet. The dimensions are shown in the mesh units (i, j) used in Forocyl. The variables

$$\begin{cases} \xi = -N\theta/2\pi \\ \eta = N_3/2\pi r \end{cases} \tag{12}$$

are used in Forocyl for radial sector machines. The total number of mesh units horizontally is a. Then

$$\begin{cases} i = a\xi \\ j = a\eta \end{cases} \tag{13}$$

(where the unit mesh is a square) are the mesh coordinates. The boundary values are shown on the diagram. The backwinding return currents are of zero cross-sectional area and are located at the points where the potential changes discontinuously. The quantity Ω calculated by Forocyl is related to the magneto-static potential ψ by

$$\psi = \left(r/r_0\right)^{k+1} \Omega . \tag{14}$$

Values of σ (phase change per sector), $\nu = N\sigma/2\pi$ (number of waves per revolution) and stability limits for radial (x) and vertical (z) oscillations are shown in Table I for different values of the relative excitation of the two

magnets of Fig. 1, given as $\Omega_1 / \Omega_1 + \Omega_2$. All of these meshes

have k = 9.3. The stability limits shown are those without misalignments. They

are given in terms of $x = r/r_0 - 1$ and $y = z/r_0$ and are simply half the

horizontal distance across the phase region of stability. The vertical stability

limit is measured with a radial motion of small amplitude.

TABLE I

Results of Exploratory Problems

I.D. Symbol	Mesh No. *	$\dfrac{\Omega_1}{\Omega_1 + \Omega_2}$	$\dfrac{\sigma_x}{\pi}$	$\dfrac{\sigma_z}{\pi}$	ν_x	ν_z	Radial Stability Limit	Vertical Stability Limit
ϵ	42	0.5	0.7956	0.6653	6.364	5.322	0.019	0.014
ϵ'	46	0.55	0.6015	0.4311	4.812	3.449	0.027	0.022
ϵ''	47	0.58	0.5454	0.3143	4.363	2.514	0.038	0.024
ϵ'''	48	0.60	0.5197	0.2375	4.158	1.900	0.027	0.025

The stability limits are measured at $\theta = 0$ (center of positive magnet). Since

this is a defocusing magnet for vertical motion, the maximum vertical amplitude

is greater than the figure given by a factor which varies from about 2 for ϵ

(due to its high σ_z) to about 1.3 for ϵ''' .

ϵ is a two-way machine, since $\Omega_1 = \Omega_2$. Its stability limits are

smaller than those for one-way machines (due to the very high $\sigma's$), but are

comparable with those of other two-way machines with N = 16. In addition, ϵ

is well situated with regard to misalignment resonances and thus appears to offer

---

*The mesh numbers are given for convenient reference by the authors and may
be regarded by the reader as cabalistic symbols.

an interesting design choice.

It is not necessary to choose a unique one-way operating point, since the accelerator can be tuned at will. It can be seen from Table I that reasonable operating points exist. The point ϵ'' appears to be the best choice from the standpoint of stability limits. Its horizontal stability limit is approximately the maximum to be expected with $\pi/2 < \sigma_x < 2\pi/3$. Its vertical stability limit is about 3/5 of the magnet aperture (y = 0.039) at $\theta = 0$, so that with a "beat factor" of at least 1.3 it clearly uses practically all of the available vacuum tank aperture. The vertical stability limit might well increase with decreasing σ_3, but the useful phase space area will not be larger. ϵ'' does not at first sight appear to be well situated with regard to misalignment resonances, since ν_3 is close to 2.5, but it should be remembered that half-integral resonances are very narrow,[3] and that the inclusion of backwinding return current effects can be expected to move ν_3 from this resonance.

VI. Misalignment Studies

One of the most important criteria in the choice of a design and operating point of an FFAG accelerator is its response to misalignments. If the stability limits of Table I become very small with only moderate misalignments, it becomes exceedingly difficult, if not impossible to achieve high beam intensities. The digital computer can be used to investigate these effects by means of transformations which simulate misaligned portions of the accelerator.

The meshes discussed above were used to study the effects of misalignments. The major effort used the "Fumblebumps" program,[10] which makes a transformation of the coordinates by amounts Δx, Δp_x, Δy and Δp_y after η integration steps. After η' steps a second such transformation (usually the inverse of the first) is made. Both transformations repeat every η_B steps and both are expressed as power series in the variables with arbitrary coefficients. Radial or vertical displacements and twists about any except the θ-axis* of any group of magnets can be simulated by these transformations. It might be noted that this also changes k and produces equivalent non-linear bumps.

In Table II stability limits are shown for ϵ and for a point δ (Mesh 40) which differs from ϵ only in having k = 9.0. Point δ has ν_x = 6.208, ν_z = 5.404. A point γ with k = 9.7 (Mesh 37, ν_x = 6.576, ν_z = 5.216) was investigated, but is not shown because its stability limits were extremely small. In each case the radial and vertical stability limits are shown. The bump size given is entered in the Formesh program scaled by r = 150 cm (so that the data correspond to a larger bump at larger radii), and one sector out of 16 is displaced or twisted. Runs of length 15 revolutions were used.

---

*This restriction occurs because Δx and Δp_x do not depend on y and p_y and Δy and Δp_y do not depend on x and p_x.

TABLE II

Stability Limits with Misalignments for Two-Way Machines

	δ		ϵ	
	Radial Stability Limit	Vertical Stability Limit	Radial Stability Limit	Vertical Stability Limit
Unperturbed	0.017	0.016	0.019	0.014
$\triangle y = 1mm$	0.017	0.012	0.011	0.012
$\triangle y = 2mm$	0.017	0.012	0.011	0.009
$\triangle x = 1mm$	0.004	0.009	0.013	0.012
$\triangle x = 2mm$	$\cong 0$	$\cong 0$	0.007	0.009
x twist (1mm)	0.004	0.010	0.012	0.012
y twist (1mm)	0.015	0.012	0.011	0.012

The data show that δ is very sensitive to radial displacements or twists, probably because it is closer than ϵ to the integral resonance $\nu_x = 6$.

The one-way machines ϵ'' and ϵ''' were investigated in the same way. Table III gives the results for these Meshes.

TABLE III

Stability Limits with Misalignments for One-Way Machines

	ϵ''		ϵ'''	
	Radial Stability Limit	Vertical Stability Limit	Radial Stability Limit	Vertical Stability Limit
Unperturbed	0.038	0.024	0.027	0.025
$\Delta y = 1mm$	0.038	0.020	0.021	0.025
$\Delta y = 2mm$	0.037	0.020	0.015	0.025
$\Delta x = 1mm$	0.037	0.020	0.021	0.025
x twist (1mm)	0.041	0.020	0.026	0.020
y twist (1mm)	0.036	0.020	0.020	0.020

ϵ''' is less favorable than ϵ'', mainly in its radial stability limits, probably because it is closer to the integral resonance $\nu_x = 4$.

It thus appears that both two-way and one-way machines have stability limits with displacements or twists of the order of a millimeter which will not inhibit beam intensity to any great degree. An equivalent field inhomogeneity would be of order 1%.

The "Mumblebumps" program[10] was also used to test the sensitivity of two-way machines to errors in azimuthally averaged field (g_0 of Eq. (6)). This program allows the introduction of a second field mesh after n_{IN} integration steps; after $n_{OUT} - n_{IN}$ more steps the program returns to the normal mesh. It was found with Mesh 42 that the radial stability limit is reduced essentially to zero if the second mesh, which is used for one sector out of 16, has $g_0 \geqslant 0.01 g_1$. Closer investigation showed that this is due

-14-

to the large tuning effects of g_0 ; the introduction of even this small g_0 had moved the radial frequency across the integral resonance $\nu_x = 6$. It was found further that small amounts of k tuning, which is to be incorporated in the accelerator, would compensate this tuning effect completely.

It may be argued that the effects of misalignments have not been tested on the final meshes with currents. However, analytical work has shown that response to misalignments depends mainly on the differences of the tune (ν_x and ν_z) from resonant values, so that currents should introduce no difficulty if the tune is not close to some harmful line.

We conclude that misalignments present no serious difficulties for the operation of the accelerator if the tolerance on misalignments is held below a millimeter.

This report does not cover the results of the investigation of the dynamical effects of the radial field ripple due to the embedding of the pole-face back-winding currents in slots cut azimuthally in the poles. These effects, which appear to be very small, are reported separately.[15]

VII. Final Meshes with Currents

In order to avoid extremely large pole-face backwinding return currents, which would reduce greatly the straight section length available for rf. devices, it is planned that the outermost part (roughly 15 cm) of the field variation will be made with non-scaling poles, the design of which is discussed in Sec. VIII. Preliminary calculations of currents in the scaling region by R. O. Haxby showed that the return bundle of pole-face windings will have cross-sectional

area of approximately 80 cm^2 at 190 cm, the end of the scaling region, where it is greatest. A geometry as shown in Fig. 2 was devised to accommodate this area. The inclusion of currents in the Forocyl program is discussed by Laslett.[16] Table IV shows the betatron oscillation frequencies obtained at different operating points with this geometry and k = 9.3.

TABLE IV

Betatron Frequencies of Operating Points with Currents

	Mesh No.	$\frac{\Omega_1}{\Omega_1 + \Omega_2}$	$\frac{\sigma_x}{\pi}$	$\frac{\sigma_3}{\pi}$	ν_x	ν_3
ϵ	146	0.5	0.79499	0.66763	6.3599	5.3410
ϵ'	147	0.55	0.59278	0.41620	4.7422	3.3296
ϵ''	145	0.58	0.53550	0.29049	4.2840	2.3239

For a field varying as r^k, the size of the backwinding return bundle does not scale, which introduces a change of frequency with radius. To find the magnitude of this effect, Forocyl meshes were run with the current bundle shrunk to zero cross-sectional area and located at point A of Fig. 2, which gives an overestimate of the effect at injection, since there must be some windings at radii smaller than the injection radius in order that the field be good at that radius. Only points ϵ and ϵ'' were tested in this way; the effect for ϵ' (or any other point between ϵ and ϵ'') obviously lies between those for ϵ and ϵ''. For a two-way operating point, such a Forocyl (Mesh 87) gives

$$\nu_x = 6.360$$
$$\nu_3 = 5.342,$$

which are indistinguishable from ϵ with currents. For ϵ'', such a Forocyl (Mesh 88) gives

$$\nu_x = 4.315$$

$$\nu_3 = 2.400.$$

Thus $\Delta\nu_x \lesssim 0.04$ and $\Delta\nu_3 \lesssim 0.08$, so that the tune change is small compared to the distance between resonances.

Data pertinent to the fields and orbits in the scaling region at ϵ, ϵ' and ϵ'' are collected in the appendix.

VIII. Design of the Non-Scaling Pole

For a given Forocyl, curves of constant Ω may be calculated by the Equicyl program.[17] Some are shown in Fig. 3. The gap height as a function of radius can be calculated as follows. At a given θ,

$$\Omega = \Omega\,(3/r)$$

or

$$3/r = g\,(\Omega) \tag{15}$$

is a function of Ω which can be evaluated numerically from Equicyl or Forocyl data. If it is assumed that the permeability of the iron is infinite, then the iron surface is an equipotential (Ψ = const.). If the gap as a function of radius is given by

$$3 = rg\left(\Psi\,(r_0/r)^{k+1}\right), \tag{16}$$

and if the pole shape at any radius is chosen to be the Equicyl curve which has the 3 of (16) at that radius, then the field scales with radius, i.e., it has the form (6) with constant k and g_n.

A pole following the exact contours of Fig. 3 would be difficult to machine. It is therefore interesting to consider whether some simpler surface gives a good approximation to the field. To do this problem with any accuracy, a finer mesh than that used for the scaling region (a = 50) must be used. Because of program limitations, there is then not enough memory space for the currents of Sec. VII. The image calculations of Weinberg[18] show that the potential varies very nearly linearly as one proceeds around the periphery of a current. This procedure was checked, with resulting ν's and fixed point x_f (position of the equilibrium orbit at $\theta = 0$) shown in Table V.

TABLE V

Check of Interpolation Method in Forocyl

	x_f	ν_x	ν_z
ϵ with Currents	-0.0100604	6.3601	5.3867
ϵ Interpolated	-0.0100528	6.3601	5.3850
ϵ'' with Currents	-0.00111303	4.3539	2.5170
ϵ'' Interpolated	-0.00127324	4.3569	2.5232

(These results are for a different geometry than the meshes of Sec. VII and therefore should not be compared invidiously with Sec. VII.)

The radius of the fixed point is $r_0 (1 + x_f)$ at $\theta = 0$, so that the differences in x_f should be compared to unity. It can be seen from Table V that the differences in dynamics are extremely small. Therefore the interpolation method was used throughout to investigate pole-shape effects.

It was found that poles of very simple cross-sectional aspect give very close fits to the frequencies for the two-way machine. It is safe to assume that all of the dynamics agrees well, since non-linear effects depend most strongly on linear frequency.

All of the pole shapes can be characterized by the parameters shown in Fig. 4. Only half a pole is shown, since each pole is symmetric about its midpoint and since positive and negative poles are alike. Boundary values are interpolated around the current bundle from $(i_b, 21)$ to $(27, 36)$, then across the straight section. Since the equipotential surfaces are not the same for different magnet excitations, there will be some change of frequency with radius in a one-way machine. Table VI shows frequencies for ϵ and ϵ'' resulting from various configurations.

TABLE VI

Linear Frequencies of Non-Scaling Poles

Mesh No.	j_o	i_a	i_b	j_b	ϵ		ϵ''	
					ν_x	ν_3	ν_x	ν_3
69	8	21	27	14	6.360	5.399	4.365	2.550
102	8	16	26	13	6.360	5.325	4.375	2.537
127	8	17	27	13	6.360	5.348	4.369	2.534
103	10	15	25	15	6.360	5.319		
104	10	15	23	14	6.360	5.308		
105	10	17	25	14	6.360	5.347		
106	10	16	26	15	6.360	5.338	4.343	2.462
121	12	16	26	17	6.360	5.345	4.312	2.392
128	12	16	22	15	6.360	5.322	4.326	2.418
137	12	17	23	15	6.360	5.339	4.316	2.411
Scaling					6.360	5.341	4.284	2.323

The variation among the fixed points for all these meshes is small com-
pared to unity, so that the scaling of momentum with radius is assured.

It can be seen that the shape of the non-scaling pole makes little difference
in the two-way case. Even the small variation of ν_z can be minimized by
a proper choice of shape. The shapes have been chosen so the vertical side
of the non-scaling pole $((i_b, j_b)$ to $(i_b, 21)$ in Fig. 4) is a single plane, as is the
slanting piece $((i_a, j_a)$ to $(i_b, j_b))$ for simplicity in machining. The boundary
between these planes is a straight line which has been chosen as horizontal
(parallel to the median plane). This uses Mesh 137 at $j = 12$, Mesh 106 at $j = 10$
and Mesh 127 at $j = 8$. In this case the change of frequency $\Delta \nu < 0.01$ in
each dimension, which is quite negligible.

If the pole is constructed in this way, the frequency changes of one-way
machines are much more serious. At ϵ'', $\Delta \nu_z > 0.2$ waves and
$\Delta \nu_x \cong 0.1$ waves. There are in addition some non-scaling terms
(derivatives of Fourier coefficients with respect to radius) which affect the
frequencies. These terms vanish with the correct non-scaling pole, because
there the Fourier coefficients are essentially independent of radius.

This difficulty can be minimized by cutting wedges from the vertical side
pieces of the non-scaling poles of the negative magnets. These pieces are of
course to be restored for two-way operation. The wedges change i_b to $i_b - \Delta i_b$
on both sides of the negative magnet of each sector (they also change j_b to
$j_b - \frac{1}{2} \Delta i_b$, since the angle $\Delta \psi$ between i_a and i_b has been chosen such
that $\tan \Delta \psi = \frac{1}{2}$).

-20-

Table VII shows the effects of various cuts on the frequencies of ϵ''.

TABLE VII

Effect of Cuts from Non-Scaling Poles

Mesh No.	Parent Mesh	j_0	Δi_b	ν_x	ν_z
112	102	8	4	4.241	2.186
122	102	8	2	4.306	2.368
113	106	10	4	4.201	1.922
124	106	10	2	4.274	2.299
138	137	12	2	4.258	2.242

If an amount $\Delta i_b = 2.484$ is cut from Mesh 102, there is no change of ν at ϵ'' at this radius. Δi_b should decrease with radius, as can be seen from the $j = 10$, 12 data. Calculation shows that if Δi_b increases uniformly from zero at the beginning of the non-scaling pole the change of frequencies is less than 0.02 in both dimensions. The non-scaling terms are extremely small since g_n is now essentially independent of r.

Since the pole as designed does not follow exactly the equipotential surfaces, the gap height as a function of radius must be modified from that given by (16). Ω is an odd function of z/r, so that

$$\Omega(z/r) = a_1(z/r) + a_3(z/r)^3 + a_5(z/r)^5 + \cdots . \tag{17}$$

a_3 gives at most a 1% correction, while a_5 is quite negligible. To give a field in the median plane which varies exactly as r^k, a_1 must be normalized to the same value for all radii (since the median plane field is completely determined by a_1). Values of a_3 normalized to $a_1 = 5.16142$ (from the scaling case) for various meshes are shown in Table VIII.

TABLE VIII

Cubic Coefficient of Potential Expansion for Various Meshes

Mesh	j_o	$- a_3$
Scaling (144)	15	44.395
102	8	68.791
127	8	70.564
103	10	54.484
104	10	55.907
105	10	64.161
106	10	61.065
121	12	57.088
128	12	49.304
137	12	54.513

The scaling mesh was used to find an approximate $j(r)$. Then this $j(r)$ was used together with appropriate meshes (128, 104, 127) to give a_3 (x), which was approximated by a power series

$$- a_3 = C_0 + C_1 x + C_2 x^2 \qquad (18)$$

The values

$$\begin{cases} C_o = 44.395 \\ C_1 = 448.795 \\ C_2 = -994.726 \end{cases}$$

were found. Then a_3 was calculated for various radii from (18). The inverted power series of (17)

$$\vartheta/r = b_1 \Omega + b_3 \Omega^3 + b_5 \Omega^5 + \cdots , \tag{19}$$

where

$$\begin{cases} b_1 = 1/a_1 \\ b_3 = -a_3/a_1^4 \\ b_5 = 3a_3^2/a_1^7 , \end{cases} \tag{20}$$

was then used to find $\vartheta(r)$. Side and plan views of the magnets are shown in Figs. 5 and 6.

Various meshes were computed to test such effects as the rounding of sharp corners to avoid saturation difficulties (Mesh 111), where the effect is found to be very small if the radius of curvature of the rounding is of order one mesh unit (with a = 150) and the effect of the relative shrinkage of the current bundle in the non-scaling region, since it is constant in size while all other dimensions scale. Mesh 126 had the current bundle shrunk by one mesh unit, but was otherwise identical to Mesh 102. Its dynamical results were essentially indistinguishable from those of 102.

Appendix

Field and Orbit Parameters

N = 16

k = 9.3

Geometry as shown in Fig. 2

TABLE IX

Fourier Coefficients of the Median Plane Fields

$$B_z = - B_0 (r/r_0)^k \sum_n g_n \cos nN\theta$$

	ϵ	ϵ'	ϵ''
g_0	0	0.5	0.66
g_1	9.635	6.278238	5.179546
g_2	0	0.107099	0.14137
g_3	-0.594694	-0.387507	-0.319693
g_4	0	-0.026192	-0.034574
g_5	-0.197399	-0.128627	-0.106117
g_6	0	0.000036	0.000048
g_7	-0.055093	0.035899	0.029617
g_8	0	0.001397	0.001844
g_9	0.004461	0.002907	0.002398
g_{10}	0	-0.000191	-0.000252
g_{11}	-0.004062	-0.002647	-0.002184

TABLE X

Field Magnitudes and Circumference Factors

Call: α_o the value of α used in computer calculations.

α_1 the value of α for which the maximum radius of the equilibrium orbit equals r_o.

α_2 the value of α for which the average radius of the equilibrium orbit equals r_o.

B_{max}/B_o is the ratio of peak field to the B_o of (6).

$C = \alpha_1 B_{max}/B_o$ is the circumference factor

The quantity $r_o B_{max}/cp$ is calculated for the maximum radius of the equilibrium orbit, i.e., α_1 is used.

	ϵ	ϵ'	ϵ''
α_o	9.635	0.5	0.66
α_1	8.70417	0.50391	0.67494
α_2	6.56152	0.404773	0.558952
B_{max}/B_o	0.923549	12.7608	8.41213
C	8.0387	6.4303	5.6777
$r_o B_{max}\left(\dfrac{\text{gauss-cm}}{\text{Mev}}\right)$	$2.6796 \cdot 10^4$	$2.1434 \cdot 10^4$	$1.8926 \cdot 10^4$

TABLE XI

Fourier Coefficients of the Equilibrium Orbits

$$x = \sum_n x_n \cos n N \theta$$

	ϵ	ϵ'	ϵ''
x_0	-0.0377277	-0.0207403	-0.0163002
x_1	0.0271438	0.0210308	0.0180896
x_2	0.0011012	0.0007277	0.0005889
x_3	-0.0003571	-0.0002158	-0.0001657
x_4	-0.0000621	-0.0000343	-0.0000266
x_5	-0.0000167	-0.0000151	-0.0000137
x_6	0.0000011	0	-0.0000002
x_7	0.0000043	0.0000030	0.0000024
α	9.635	0.5	0.66

Note: These change with α according to the relation

$$x_n' + \delta_{no} / x_n + \delta_{no} = (\alpha/\alpha')^{\frac{1}{k+1}}.$$

TABLE XII

Coefficients of the Linear Transformation Matrix

$$\begin{pmatrix} q(\theta+2\pi/N) \\[4pt] \frac{dq}{d\theta}(\theta+\frac{2\pi}{N}) \end{pmatrix} = \begin{pmatrix} \cos\sigma + \alpha_T\sin\sigma & \beta\sin\sigma \\[4pt] -\frac{1+\alpha_T^2}{\beta}\sin\sigma & \cos\sigma - \alpha_T\sin\sigma \end{pmatrix}\begin{pmatrix} q(\theta) \\[4pt] \frac{dq}{d\theta}(\theta) \end{pmatrix}$$

	ϵ	ϵ'	ϵ''	
$\cos\sigma_x$	-0.799660	-0.287383	-0.111300	
$\sin\sigma_x$	0.600453	0.957816	0.993787	
β_x (Max.)	0.97374	0.53325	0.47021	at $N\theta/2\pi = 1$ (Mod.1)
β_x (Min.)	0.050826	0.11629	0.14364	at $N\theta/2\pi = \frac{1}{2}$ (Mod.1)
β_x (St. Sect.)	0.35059	0.26895	0.27087	at $N\theta/2\pi = \frac{1}{4}$ (Mod.1) $= \frac{3}{4}$ (Mod.1)
α_{Tx} (St. Sect.)	±2.8782	±1.3783	+1.1186	(+) at $N\theta/2\pi = \frac{1}{4}$ (Mod.1) (−) " " = $\frac{3}{4}$ (Mod.1)
$\cos\sigma_z$	-0.502633	0.260225	0.611698	
$\sin\sigma_z$	0.864500	0.965548	0.791091	
β_z (Max.)	0.41585	0.46265	0.60278	at $N\theta/2\pi = \frac{1}{2}$ (Mod.1)
β_z (Min.)	0.086259	0.19365	0.30353	at $N\theta/2\pi = 1$ (Mod.1)
β_z (St. Sect.)	0.26161	0.34063	0.46747	at $N\theta/2\pi = \frac{1}{4}$ (Mod.1) $\frac{3}{4}$ (Mod.1)
α_{Tz} (St. Sect.)	∓1.3887	∓1.1070	∓1.2246	(+) at $N\theta/2\pi = \frac{3}{4}$ (Mod.1) (−) " " = $\frac{1}{4}$ (Mod.1)

In addition to the flutter tuning by which ϵ' and ϵ'' are reached from ϵ, it is planned to provide k tuning, so that radial and vertical betatron oscillation frequencies can be changed independently. Table XIII shows the effect of small changes of k at ϵ and ϵ''. These meshes do not include currents, so should be compared with 42 and 47.

TABLE XIII

Effect of Change of k on Frequencies

	Mesh No.	k	ν_x	ν_3
ϵ {	89	9.393	6.418	5.290
	90	9.486	6.464	5.266
	91	9.579	6.514	5.242
	92	9.765	6.639	5.195
ϵ'' {	93	9.393	4.398	2.490
	94	9.486	4.422	2.470
	95	9.579	4.447	2.449
	96	9.765	4.497	2.407

These results and the flutter tuning can be represented at ϵ by

$$\frac{\Delta \nu_x}{\nu_x} \cong -2.5 \frac{\Omega_1 - \Omega_2}{\Omega_1} \cong -0.8 \frac{\Delta k}{k} \; ;$$

$$\frac{\Delta \nu_3}{\nu_3} \cong -3.5 \frac{\Omega_1 - \Omega_2}{\Omega_1} \cong -0.5 \frac{\Delta k}{k} \; .$$

At ϵ'', the results can be represented by

$$\frac{\Delta \nu_x}{\nu_x} \cong -1.5 \frac{\Omega_1 - \Omega_2}{\Omega_1} \cong 0.6 \frac{\Delta k}{k}$$

$$\frac{\Delta \nu_3}{\nu_3} \cong -7 \frac{\Omega_1 - \Omega_2}{\Omega_1} \cong -0.9 \frac{\Delta k}{k}$$

References

1. T. Ohkawa, MURA-124, June 7, 1956 and T. Ohkawa and L. W. Jones, B.A.P.S., Series II, 2, 11 (1957).

2. D. W. Kerst et al., Phys. Rev. 102, 590 (1956).

3. F. T. Cole et al., Rev. Sci. Inst. 28, 403 (1957).

4. Minutes of the MURA Technical Group Staff Meeting #16, January 28, 1957.

5. L. J. Laslett and J. N. Snyder, MURA-221 (Internal), February 28, 1957.

6. L. D. Fosdick, MURA-226 (Internal), February 28, 1957.

7. J. L. Powell, MURA-80, August 16, 1955.

8. L. J. Laslett and J. N. Snyder, MURA-222 (Internal), February 28, 1957.

9. J. N. Snyder, MURA-231 (Internal), February 28, 1957.

10. J. N. Snyder, MURA Reports Number 234, 235, 236 all internal and dated February 28, 1957 and MURA-328 (Internal), July 1, 1957.

11. L. D. Fosdick, MURA-241 (Internal), March 1, 1957.

12. The parameter α was first introduced by Ohkawa (Minutes of the MURA Technical Group Staff Meeting #6, November 12, 1956).

13. See T. Ohkawa, MURA-318, July 5, 1957, for the two-way case.

14. K. R. Symon et al., Phys. Rev. 103, 1837 (1956).

15. M. J. Freiser and A. M. Sessler, MURA-366 (Internal), October 21, 1957.

16. L. J. Laslett, MURA-211 (Internal), December 4, 1956.

17. J. N. Snyder, MURA-230 (Internal), February 28, 1957.

18. E. Weinberg, MURA Notes, June 30, 1956.
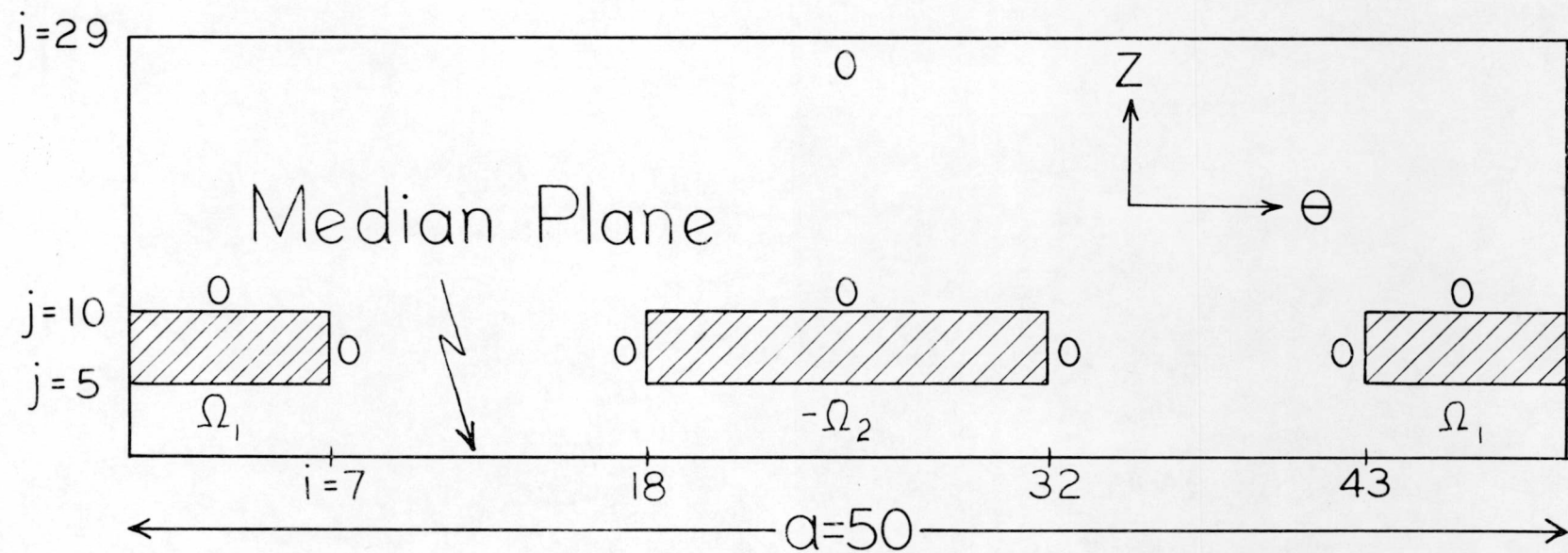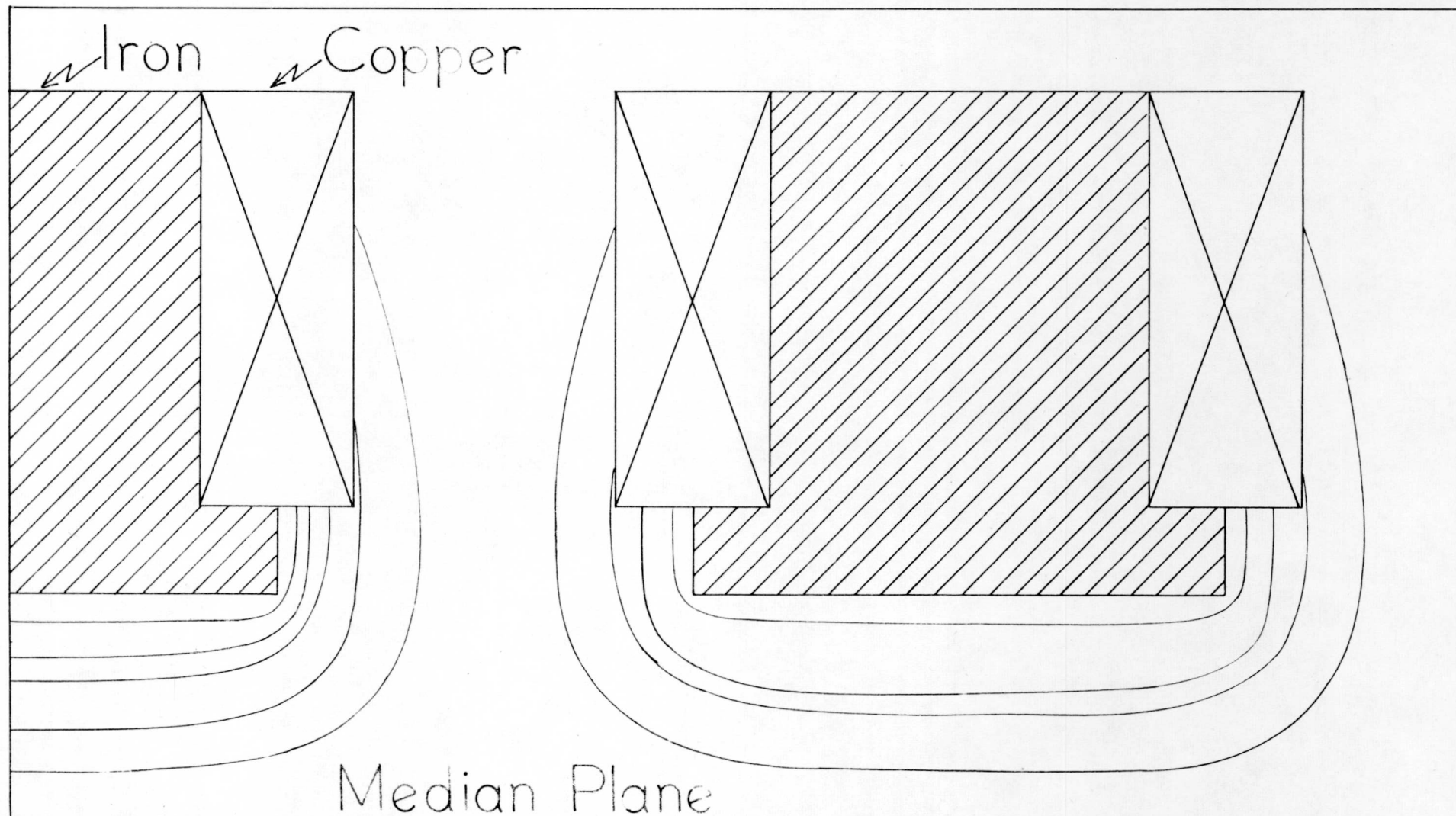
Pole Geometry of a Forocyl Problem

Fig. 1

Final Pole Geometry with Currents

Fig. 2
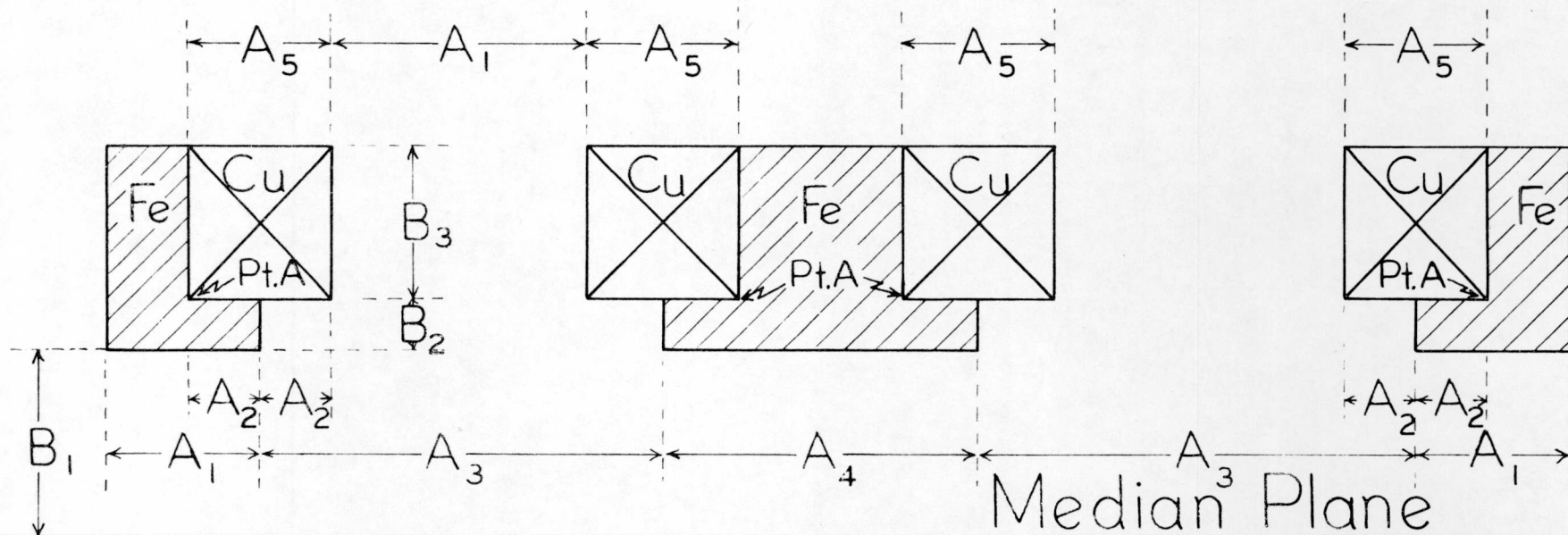
$A_1 = .0549779$
$A_2 = .01570796$
$A_3 = .0863938$
$A_4 = .1099557$

$A_5 = .03141593$
$B_1 = .03926991$
$B_2 = .01570796$
$B_3 = .07068584$

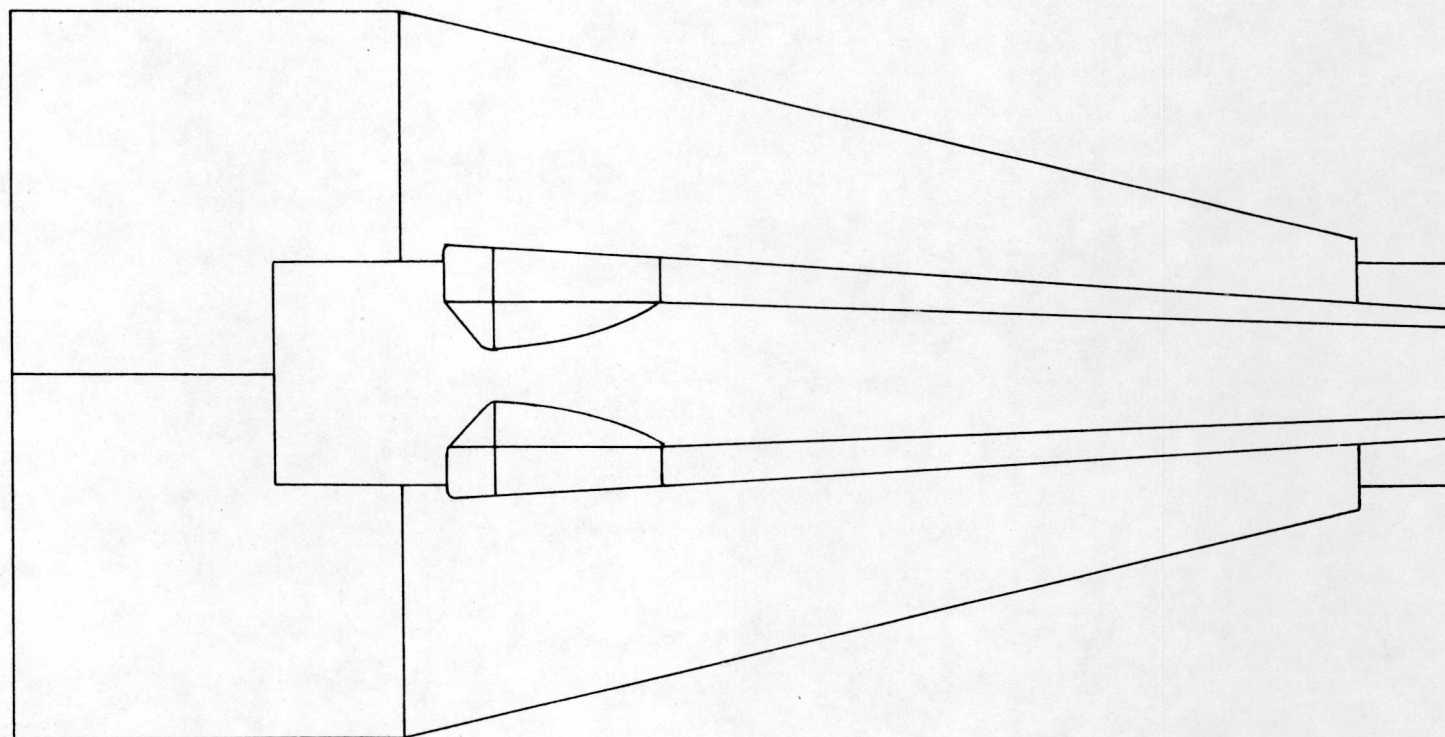Dimensions in units of radius

Iron   Copper

Median Plane

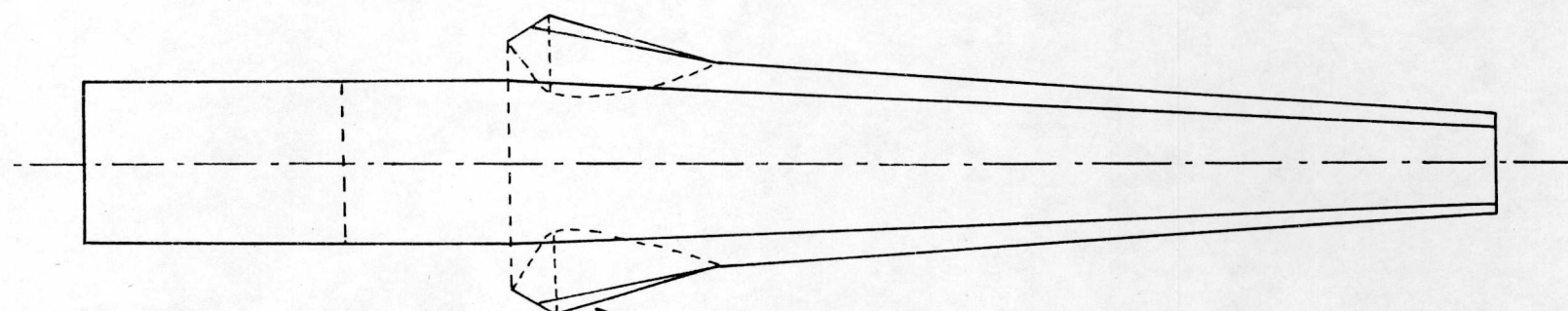Magnetostatic Equipotentials for Two-Way Tuning
Fig. 3
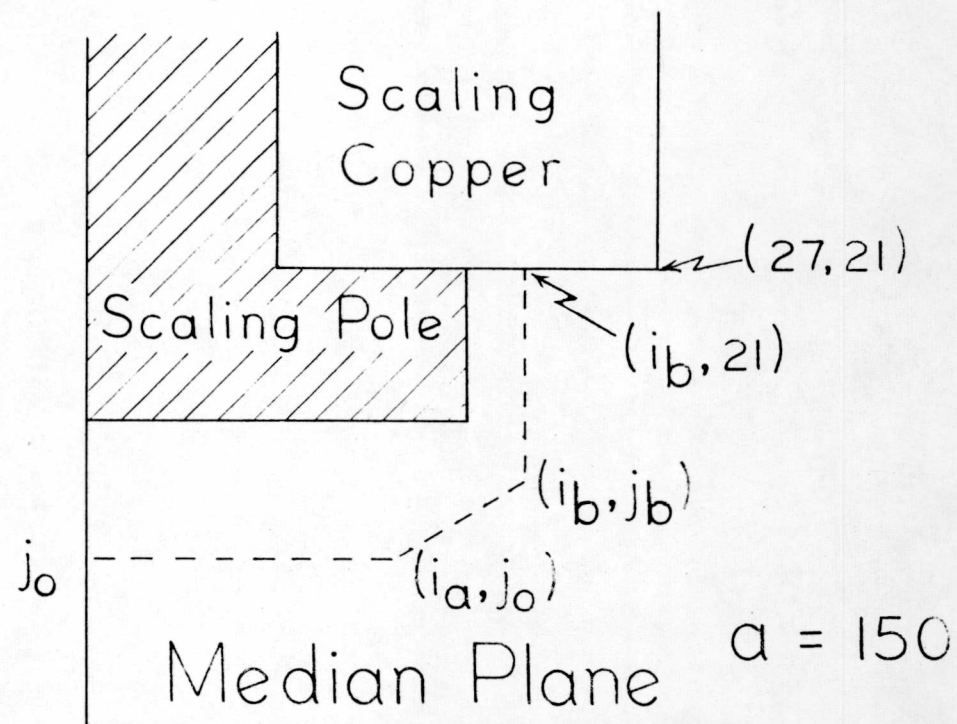
Scheme of Approximations to Non-Scaling
Poles.

Fig. 4

Side View of Magnet

($\frac{1}{8}$ scale - Current Slots not shown)

Fig. 5

Non-Scaling Pole

Plan View of Magnet

($\frac{1}{8}$ scale, current slots not shown)

Fig. 6